Journal of Electron Spectroscopy and Related Phenomena 202 (2015) 26–32

Contents lists available at ScienceDirect

Journal of Electron Spectroscopy and Related Phenomena

journal homepage: www.elsevier.com/locate/elspec

Analysis of multi-layer ERBS spectra

G.G. Marmitt[a,b], L.F.S. Rosa[b], S.K. Nandi[c,d,e], M. Vos[a,*]

[a] Atomic and Molecular Physics Laboratories, Research School of Physics and Engineering, The Australian National University, Canberra 0200, Australia
[b] Instituto de Fisica da Universidade Federal do Rio Grande do Sul, Avenida Bento Goncalves 9500, 91501-970 Porto Alegre, RS, Brazil
[c] Electronic Materials Engineering Department, Research School of Physics and Engineering, The Australian National University, Canberra 0200, Australia
[d] Research School of Astronomy and Astrophysics, The Australian National University, Canberra, ACT 2611, Australia
[e] Department of Physics, University of Chittagong, Chittagong 4331, Bangladesh

ARTICLE INFO

Article history:
Received 21 January 2015
Received in revised form 13 February 2015
Accepted 14 February 2015
Available online 21 February 2015

Keywords:
Electron Rutherford backscattering
Surface analysis
Depth profiling

ABSTRACT

A systematic way of analysis of multi-layer electron Rutherford backscattering spectra is described. The approach uses fitting in terms of physical meaningful parameters. Simultaneous analysis then becomes possible for spectra taken at different incoming energies and measurement geometries. Examples are given to demonstrate the level of detail that can be resolved by this technique.

1. Introduction

Electron Rutherford backscattering (ERBS) is a technique that depends on the recoil energy transferred from the scattering electron to a nucleus in a large-angle deflection. This energy transfer depends on the mass of the scattering atom. Analysing the energy of the scattered electrons reveals thus which atoms are present in the near surface layer [1,2].

In simple cases where there are 2–3 separate peaks due to different elements that do not overlap one can simply fit the spectra with the corresponding number of Gaussians. In more complicated cases the peaks overlap and an unique fitting of the spectrum based on a larger number of Gaussians cannot be obtained. Position, width and relative intensity of the different Gaussians should be constrained based on theory and/or the measurement of reference samples consisting of pure materials. In the case of the analysis of the elemental composition of mouse bones we proceeded along these lines [3]. Here we want to follow a similar approach for the study of samples consisting of layers of different composition. Besides the composition of each layer it is then of interest to measure their thickness. The added complexity will usually require the measurement of the sample under different geometries and/or incoming energies and the simultaneous analysis of all spectra. As we will show here, fitting of the data allows for very precise thickness determination, provided that the most of the parameters are based on physics. The accuracy of the thickness measurements is limited by the knowledge of the inelastic mean free paths (IMFP) for the different layers. Conversely, if the thicknesses are known these experiments can be used to determine the IMFP experimentally.

In the above we assumed that the sample can be described as a homogeneous overlayer. If this is not the case (e.g. overlayer consists of islands, or significant inter-diffusion of substrate and overlayer) then the interpretation of the results of different measurements taken at different energies and/or geometries in terms of homogeneous layers, will result in inconsistent results. Here we mainly discuss the simple case where the overlayer is expected to be quite homogeneous in thickness and composition.

In the rest of this paper we describe the fitting procedure in some detail, and then give some actual examples. We first analyse a simple case of a carbon film deposited on Au, where the peaks do not overlap. Subsequently we study the case of a Si_3N_4 layer on TiO_2, where the peaks overlap strongly, and show that highly consistent estimates of the thickness of the Si_3N_4 film are obtained for different measurement geometries.

Finally we study the case of Xe implanted TiO_2. Here the Xe implantation affects the stoichiometry (preferential sputtering of O in the TiO_2 film). By assuming a very simple model for the Xe intensity distribution and O depletion we find that our combined data set can be described by assuming a finite implantation depth of the Xe and O depletion due to preferential sputtering that extends well below the outermost surface layer.

* Corresponding author. Tel.: +61 2 6125 4985.
E-mail address: maarten.vos@anu.edu.au (M. Vos).

http://dx.doi.org/10.1016/j.elspec.2015.02.009
0368-2048/

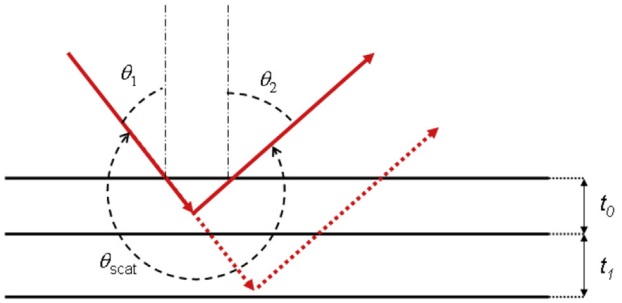

Fig. 1. Interpretation of an electron Rutherford backscattering experiment assuming v-shaped trajectories.

2. Theory

The incoming electron (energy E_0, momentum $\boldsymbol{k}_0$) is deflected by elastic scattering from nuclei in the target material. We assume v-shaped trajectories, i.e. there is for each detected electron only one large-angle elastic scattering event. The scattering angle of that event (θ_{scat}) is taken to be the angle between the incoming beam and the outgoing electrons that are detected in the analyser with momentum $\boldsymbol{k}_1$. The magnitude of the momentum transfer $\boldsymbol{q} = \boldsymbol{k}_0 - \boldsymbol{k}_1$ in the elastic collision is then given by $q = 2\ \boldsymbol{k}_0 \sin(\theta_{\text{scat}}/2)$ as $|k_0| \approx |k_1|$.

The sample is considered to be composed of different layers n with thickness t_n. The intensity of the contribution of element i in the outermost layer ($n = 0$) is proportional to:

$$I_{i,0} = \gamma\, C_{i,0}\, \sigma_i\, \lambda_0\, (1 - e^{-t_0^{\text{eff}}/\lambda_0}). \tag{1}$$

The intensity of element i in the second layer is given by a similar expression as Eq. (1) but now attenuated by a factor due to inelastic scattering of the incoming and outgoing beam in layer 0:

$$I_{i,1} = \gamma\, C_{i,1}\, \sigma_i\, \lambda_1\, (1 - e^{-t_1^{\text{eff}}/\lambda_1})\, e^{-t_0^{\text{eff}}/\lambda_0}. \tag{2}$$

Here γ is a constant related to the spectrometer opening angle and efficiency, integrated beam current, measurement geometry, etc. and will not affect the shape of the spectrum. t_j^{eff} is the effective thickness of layer j (or, more precisely, the total path length of the electrons that transverse layer j completely, i.e. $t_j^{\text{eff}} = t_j * (1/\cos\theta_1 + 1/\cos\theta_2)$ with θ_1 and θ_2, the angle of the incoming and outgoing trajectories with the surface normal (see also Fig. 1). $C_{i,j}$ is the concentration of element i in layer j. σ_i is the differential scattering cross section of element i at θ_{scat} and energy E_0; λ_j is the inelastic mean free path of electrons with energy E_0 in layer j. For a three-layer sample the intensity of the third layer would be similar to that given in Eq. (2) except for an additional factor $e^{-t_1^{\text{eff}}/\lambda_1}$ describing the attenuation in the second layer.

The differential elastic scattering cross section (DCS) for the given geometry and incoming electron energy is thus a required input parameter. This is an atomic property that is not thought to be affected by the fact that the atoms are here part of a solid. It can be either calculated using, e.g. ELSEPA [4,5], or conveniently retrieved using the NIST database (http://www.nist.gov/srd/nist64.cfm), which is based on ELSEPA. Accuracy here is thought to be of the order of 5%. The main uncertainty is how absorption (the reduction in the number of elastically scattered electrons due to the presence of inelastic loss channels) should be treated [4,5]. In the NIST data base absorption is not considered. Calculating the DCS with absorption ELSEPA reduces the DCS of C by 1% and for Au by 4% for our conditions ($E_0 = 40$ keV, $\theta_{\text{scat}} = 135^\circ$). Thus absorption could affect the ratio of the DCS of a light and a heavy element by about 3%.

The second input parameter is the inelastic mean free path (IMFP) λ_i. Here most theoretical and experimental results are for lower energies (XPS range, around 1 keV). Extrapolating the results of the TPP-2M formula ([6], designed for kinetic energies up to 2 keV) to 40 keV is often the most convenient approach. For a limited number of solids values have been calculated up to 30 keV, based on optical data [7]. Comparing the values calculated at 30 keV with those obtained from TPP-2M formula one gets agreement at the level of 20% or better [7], with the exception of carbon-based materials where the discrepancy is larger. The level of agreement between both theories does not change significantly if the energy is changed from 2 keV to 30 keV.

The main uncertainty in the analysis of ERBS experiments of samples with a homogeneous overlayer is thus due to the inelastic mean free path, rather than the elastic scattering cross section and can be of the order of 20% when using the TPP-2M formula, and presumably significantly less if one has access to a more recent evaluation of the IMFP based on optical data.

In an actual experiment one tries to measure the layer thickness assuming the composition of the layers is known, or one assumes the thickness known and measures the layer composition. In some cases neither thickness and composition of a layer are known, and then one can try to determine both. As we will show in such a case one requires usually measurements taken in different geometries to determine both thickness and composition. If the composition is not known, then it will be more difficult to obtain an accurate estimate of the IMFP. For example, for a non-stoichiometric oxide one would use the IMFP calculated for the stoichiometric phase with a composition that is closest to the actual sample.

The contribution of an element (mass M_a) to the spectrum is not simply positioned at the recoil energy loss for scattering from a stationary atom: $E_{\text{rec}}^{\bar{i}} = q^2/2M_a$, but spread out over a Gaussian distribution due to the energy resolution of the spectrometer and Doppler broadening due to atomic vibrations. For our set-up, using slit lenses, the scattering angle is well defined ($\Delta\theta \approx 0.2^\circ$) and the finite opening angle contributes very little to the observed width. For all but the heaviest elements the width of this distribution is dominated by Doppler broadening rather than the energy resolution of the spectrometer. For isotropic materials this Doppler width is given by [8]:

$$\sigma_i = \sqrt{\frac{4}{3} E_{\text{rec}}^{\bar{i}}\ E_{\text{kin}}^{\bar{i}}}, \tag{3}$$

where $E_{\text{kin}}^{\bar{i}}$ indicates the mean kinetic energy of atom i.

A fitting procedure of the experiment should include this broadening. Unfortunately there is no database or simple theory for $E_{\text{kin}}^{\bar{i}}$ for atoms in solids. In the case of materials with a low Debye temperature (significantly below the measurement temperature) one can approximate the mean kinetic energy by $(3/2)\,kT$ ($\approx$0.0375 eV for a room temperature measurement). In other cases the zero point motion contributes significantly to the mean kinetic energy and the mean kinetic energy will exceed this value, often by a significant amount. These ERBS experiments are one of the few ways of measuring the mean kinetic energy directly. If one wants to analyse complicated samples successfully it is often required to first measure a pure material to get a good estimate of the mean kinetic energy and keep this value fixed in the analysis of more complex samples.

3. Fitting procedure

The spectrum consists thus of a number of Gaussian peaks, with different widths and intensities, centred at different energy losses. An ERBS spectrum is thus calculated from the following input parameters related to the sample:

i *Mass of the atoms present*. Generally it will suffice to take the average mass of each element. For the lightest atoms (H, D, Li and B isotopes) it is advisable to calculate the contribution of each isotope separately, i.e. each isotope is described with a Gaussian with its own energy position and intrinsic width (both calculated from their mass). This quantity is never used as a fitting parameter.

ii *DCS for each element present*. This can be conveniently obtained from a elastic scattering database, or a partial wave calculation such as ELSEPA. Never used as a fitting parameter.

iii *Mean kinetic energy ($E^{\bar{i}}_{\mathrm{kin}}$) for each element present*. This is best obtained from a reference sample. For the reference sample this value would thus be a fitting parameter. Unfortunately there is no well-established way to calculate this property. As the width is only proportional to the square root of the mean kinetic energy, the outcome of the fit is not very sensitive to the value used. If an element is present in both substrate and overlayer, than the mean kinetic energy will generally be different for the contribution of the same element in both layers.

iv Elemental composition of the unit cell for each layer.

v *Number of unit cells per unit volume for each layer*. The easiest way to obtain this number is using the specific weight divided by the atomic mass of the unit cell. It is required to put the contribution of overlayer and substrate on the same scale. It is always a fixed parameter.

In principle the information of (iv) and (v) could be given in a single input item (number of scatterers of element x per cm^3), but we find the described way more convenient.

vi *Inelastic mean free path for each layer*. This can be obtained from calculations based on optical data (most precise) or more conveniently from the TPP-2M formula.

vii *Thickness of each layer*. Throughout most of this paper we assume that all layers have an uniform thickness.

Then there are several parameters related to the experimental set up and spectrometer performance

viii *Overall intensity scaling factor*. This factor increases as more and more counts are collected. As the efficiency of the spectrometer is not known this is always a fitting parameter.

ix *Incoming energy E_0*. This is nominally known from the high-voltage power supply settings used. It is usually a fitting parameter, as the Chi-square is strongly dependent on the exact value used here. The obtained value should differ from the nominal value by less than 1% for conducting samples. Larger deviations are either a sign of charging (for insulators) or a different sample composition from the one assumed, or both. Note that variations (ripple, drift) in the main power supply (and charging of the sample) do not show up in the energy loss scale, as the same field is used to accelerate and decelerate the electrons.

x *Zero position of the energy loss scale.* This is slightly dependent on the exact sample position (variations of the order of an eV), and is almost always a fitting parameter

xi *Energy resolution ΔE_{res}*. This describes the energy resolution as well as the thermal spread of the incoming beam and is taken to be Gaussian. It is also slightly dependent on sample position, beam current used etc., so it is a fitting parameter, but the energy resolution should always be close to 0.3 eV full width half maximum. It is only possible to derive a value of ΔE_{res} from the experiment if one assumes that the mean kinetic energy of an element causing a major peak is known. In practice we use a Au layer for, this as it is a heavy atom and a soft material (low Debeye temperature, hence the mean kinetic energy should be close to $3/2kT$).

xii *Scattering angle θ_{scat}*. This is the angle defined by the position of the gun and analyser and is always kept fixed.

xiii *Incoming and outgoing angle θ_1, θ_2*. These angles can be changed by rotating the manipulator and should always be known.

The previous parameters all have a clear physical meaning that relates to the spectrometer or the composition and thickness of the target. There is however, also a small background not related to electrons that have *only* scattered elastically. It is part due to the dark count rate of the detector and this can be easily obtained from the count rate at the negative energy loss part of the spectrum, well away from any elastic peak. More tricky to determine is the contribution of electrons that have scattered elastically *and* inelastically. It is determined mainly by the loss function of the materials involved. Additional contributions of surface and interface plasmons will contribute, but are expected to be relatively small for the large E_0 values used here.

For insulators one expects no contribution of inelastic events up to the band gap below the main elastic peak. Thus in that case the background is kept on the dark count rate level up to this value and it is usually assumed to increase linearly afterwards. For metals inelastic excitations extends all the way to zero energy loss, and then an increase in the background is expected at each elastic peak. This increase is modelled in such a way that it does not cause a discontinuity at the mean recoil energy, by taken it to be proportional to the fraction of the Gaussian distribution at lower energy loss values.

One can take a combination of both backgrounds. The guiding principle here is that the background at low energy loss values should resemble that measured for small incoming energies (e.g. $E_0 = 5$ keV or below) where recoil effects do not split up the elastic peak. Modelling of the inelastic background is critical for compounds consisting of a low and a high Z element (e.g. HfO_2), where the intensity of electrons scattered from the high-Z element (large cross section!) *plus* additional inelastic scattering can be comparable to the intensity of the elastic peak of the light element. It is less a critical issue when only lighter elements are involved.

The fitting procedure is implemented using the Origin plotting program (http://www.originlab.com) and the function (written in C) is available as part of the supplementary material of this paper. Within the Origin fitting environment parameters can be kept fixed just by ticking a box, and as many parameters as possible of the fitting function should be kept fixed. Care should be taken that two parameters that are strongly correlated are not allowed to vary simultaneously. For example one can determine the thickness of a layer if the IMFP is known and kept fixed, alternatively one can determine the IMFP if the thickness of a layer is fixed but no unique solution will be found if both parameters are free.

The Origin fitting environment makes it possible to fit two or more spectra simultaneously. The user can choose which parameters to share between both fits. We will show that this is a very useful feature to unravel more complicated cases.

4. Results

4.1. Carbon films on Au

First we will illustrate how the fitting procedure works for the case of a carbon film deposited on a Au substrate. For this experiment results, without detailed fitting, were published before [9], and the fitting procedure is not really required as the peaks do not overlap. There is a very strong dependence in the spectra on the sample orientation and E_0 values used. It is thus a good way to test

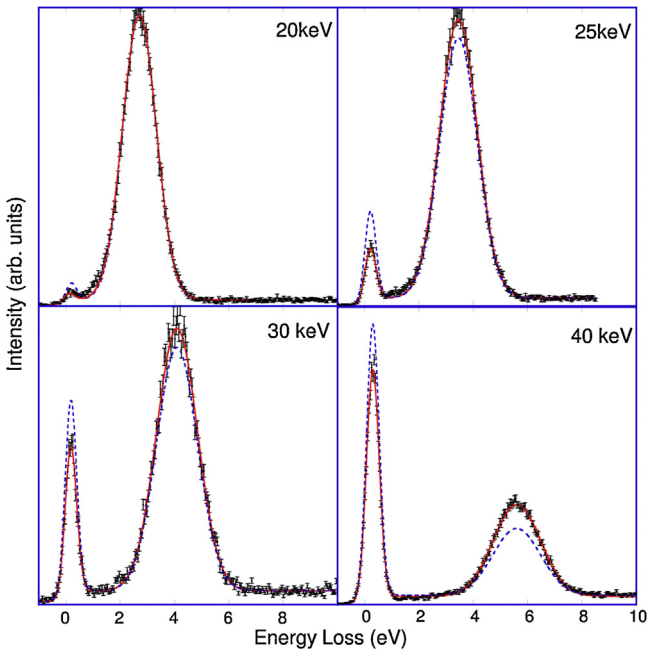

Fig. 2. Spectra of an Au sample covered by a carbon film, taken for 4 different incoming energies as indicated at $\theta_2 = 45°$. The full (red) line is a fit using the graphite mean free path as a free parameter. The blue dashed line is the best description that can be obtained if the mean free path of graphite is fixed at a value 10% larger than the value that gives the best fit. (For interpretation of the references to colour in this figure legend, the reader is referred to the web version of this article.)

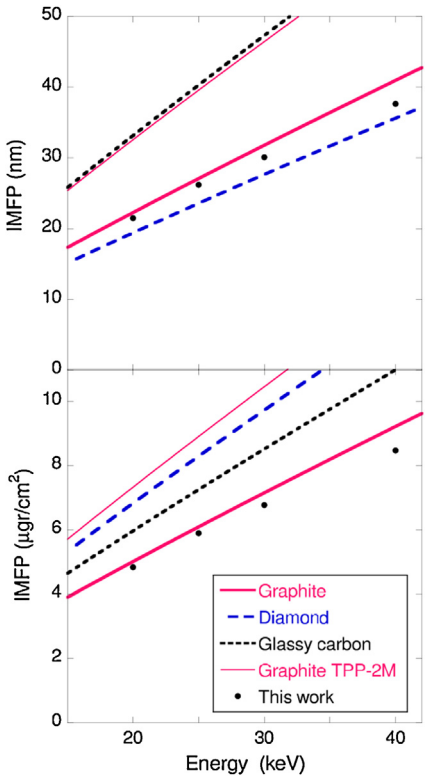

Fig. 3. The upper panel shows the energy dependence of the IMFP (in nm) as measured here for a graphite film, and as calculated for several carbon films using the approximation given in [7] which was developed for energies up to 30 keV. For graphite we show the results of the TPP-2M formula as well [11]. Experimentally our film thicknesses was given in terms of μg/cm^2. The lower panel shows the same data but now the IMFP is expressed in terms of μg/cm^2.

drive the procedure, and of interest to check the level of consistency that can be obtained in the description of the very different spectra. Note that in these somewhat earlier ERBS spectra a slightly different geometry was used (as described in Ref. [9]), the scattering angle was 120° with the gun, surface normal and analyser are not in the same plane in contrast to the data described later in this paper.

The carbon overlayer was obtained commercially from Arizona Carbon Foil Co. It is an amorphous film and has a quoted weight of 16.0 μg/cm^2. Using the density for graphite of 2.25 g/cm^3 (Quoted values of the density of graphite varies somewhat, this value is taken to be consistent with the calculations of the IMFP [7]) this corresponds to a thickness of 71.1 nm. The carbon film was floated off a microscope slide and picked up on a thick gold foil. Part of the Au was left uncovered. This uncovered part showed a single elastic peak. From energy loss measurements of these films we know that the plasmon is at a slightly lower energy loss value than for HOPG [10] and there is no peak at the π plasmon energy loss of 7 eV. These films can thus not really be described as graphite.

In Fig. 2 we show the spectra obtained from these samples for different incoming energies. The low loss peak is due to electrons scattered from Au, the broader peak at larger loss values due to electrons scattered from C. As expected the separation of the peaks is proportional to the incoming energy. The ratio of the peak areas is a strong function of the incoming energy. Qualitatively these spectra were described and understood before [9], here we want to see if the expression derived above can fit all these spectra consistently.

As mentioned before the description of the background is somewhat ad hoc. After the Au peak there is a clear increase in the background level. Hence we fitted the spectra with a constant background that increases in value near the Au peak. Such an increase is not obvious for the C peak and no step in the background was included for this element. The spectra were fitted with the mean kinetic energy of the C atoms ($\bar{E}_{kin}$) linked for the fits at the four different energies. A value of 0.098 eV was obtained, in good agreement with earlier estimates [8]. Thus by expressing the intrinsic width in terms $\bar{E}_{kin}$ via Eq. (3) we can avoid having a fitting parameter for the C width for *each* measurement. A good fit of all four spectra was obtained in this way with the mean free path as the main fitting parameter. The estimates of the mean free path obtained are shown in Fig. 3. The change in IMFP with energy is very regular, and the values found are close to those calculated for graphite [7].

It is worth noting that spectra are very sensitive to the value of the C IMFP. This is because the carbon layer is thick, and the total path length (incoming and outgoing) in the C film is at least 200 nm. That means that even at 40 keV the path lengths are 5 times the IMFP. The fact that we still see a clear Au peak is because the Au DCS is several hundred times larger than the C DCS. A mere 10% change in the C IMFP results in a very poor fit (dashed line in Fig. 2). A 10% increase in IMFP causes a change in the path length, expressed in terms of the IMFP from 5 to 4.5 at 40 keV and this corresponds to a substantial change in strength of the Au signal, by much more than 10%. From the strong dependence of the fitting results it appears that the mean free path can be determined with an accuracy of 1%.

We used for Au the IMFP as given by Tanuma et al. [7]. The value of the Au IMFP used affects the IMFP obtained for carbon. Increasing the Au IMFP by 10% over the value from Ref. [7] results only in a 1.5% decrease of the obtained IMFP for carbon. The fact that the obtained C IMFP is rather insensitive to the Au IMFP used is again due to the exponential nature of the attenuation in the C film. The present measurement configuration seems thus very favourable for the measurement of the IMFP in films of light elements on a high-Z substrate. Unfortunately for the present film it is not clear how representative it is for graphite.

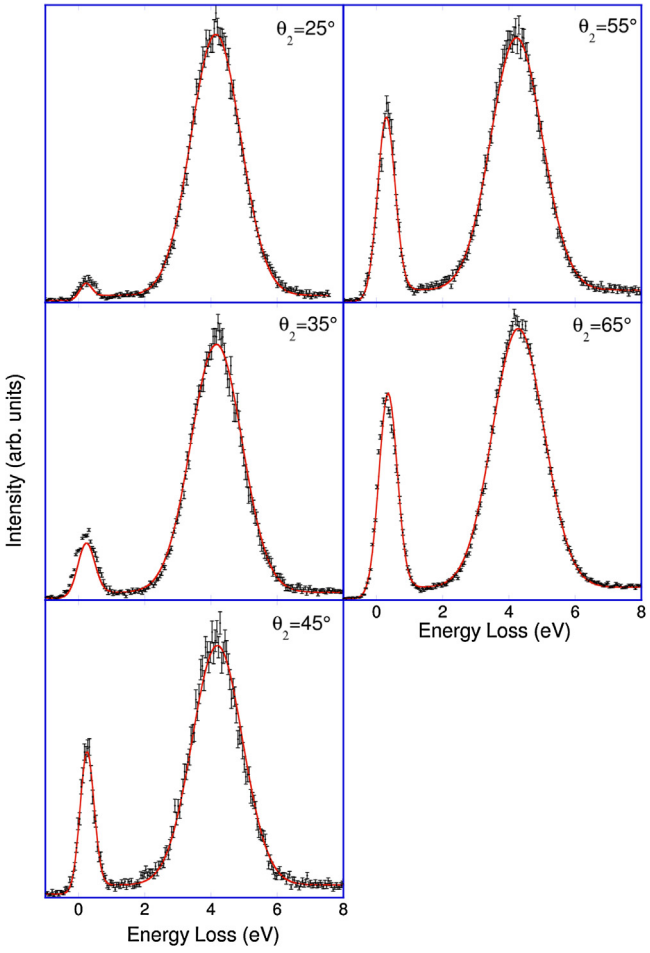

Fig. 4. Angle-dependence of the obtained spectra for the same sample as in Fig. 2 but now for different geometries as indicated by the different values of θ_2. The energy E_0 was 30 keV.

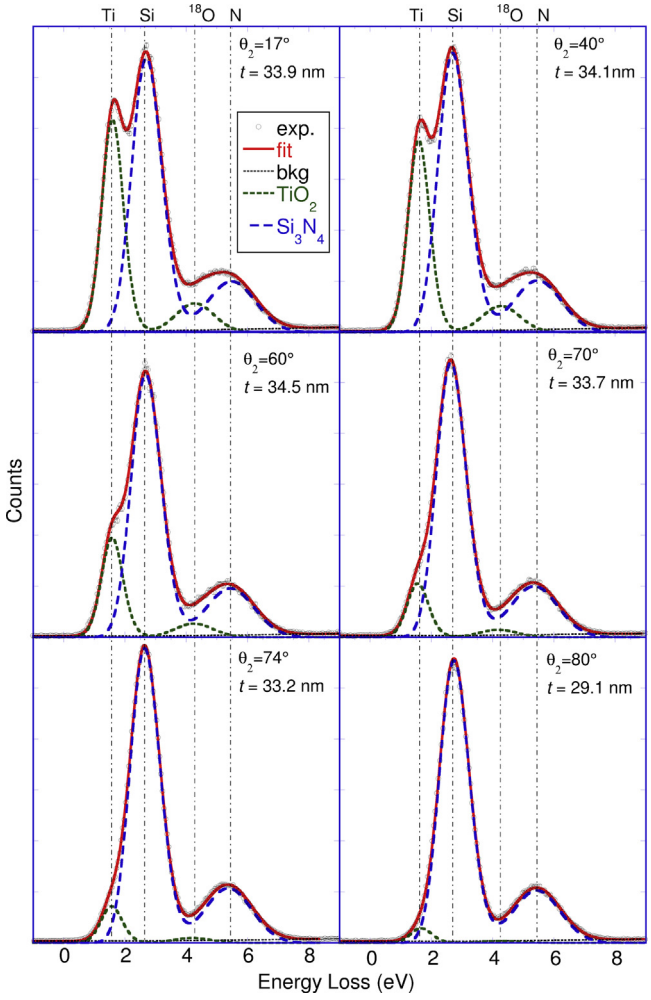

Fig. 5. The angular dependence of the spectra of 35 nm Si_3N_4 deposited on TiO_2 for different outgoing angles θ_2 as indicated. Each graph also shows the thickness of the Si_3N_4 film as determined in that geometry. The short dashed line is the TiO_2 contribution to the spectrum, the long dashed line the Si_3N_4 contribution. The energy E_0 was 40 keV.

For $E_0 = 30$ keV spectra were taken for this sample for different orientations as shown in Fig. 4. The outgoing angle was varied between 25° and 65° and again dramatic changes in the resulting spectra were found. These spectra were fitted using the IMFP in carbon as a shared variable and a value of 29.4 nm was obtained in very good agreement with the value of 29.2 nm obtained for the 30 keV measurement of Fig. 2. The large variation in the spectra with orientation is well reproduced by the fits. It is thus clear that our fitting approach describes these measurements with a high level of accuracy.

4.2. Si_3N_4 layer on TiO_2

Now we want to consider a more complicated case, where the peaks are overlapping. For this purpose we choose a Si_3N_4 film deposited on TiO_2. The TiO_2 film was 150 nm thick, exceeding the probing depth of these experiments. In the configuration used here $\theta_{scat} = 135°$ and the gun, surface normal and analyser are in the same plane. It was grown by plasma deposition using ^{18}O and intended for use in O diffusion studies. The Si_3N_4 was deposited by plasma enhanced chemical vapor deposition and the thickness was measured afterwards by ellipsometry and determined to be 37 nm. These films are known to be slightly sub-stoichiometric and may contain some hydrogen. The parameters describing the TiO_2 film were determined from the sample before the Si_3N_4 deposition and kept fixed. The Si_3N_4 parameters were determined from a fit of the spectrum with $\theta_2 = 80°$ where the TiO_2 component was only a minor contribution. From this measurement we obtain a stoichiometry of $Si_3N_{3.7}$ and this value was used in all subsequent fits. The IMFP values used in the fit were those obtained from the TPP-2M formula (52.7 nm at 40 keV for Si_3N_4 and 45.1 nm for TiO_2). All spectra were fitted simultaneously with the thickness as a shared parameter, and a value of 33.8 nm was obtained for the film thickness in this way. The spectra were also fitted separately with the thickness determined independently for each geometry and these results are shown in the panels of Fig. 5. Clearly the internal consistency of the thickness measurement is very good, with larger but still modest deviations occurring for geometries where the TiO_2 contribution to the spectrum becomes very small.

The thickness measured in this way is about 10% smaller than the thickness obtained by ellipsometry. Adopting the ellipsometry thickness and fitting the Si_3N_4 IMFP we obtain an IMFP at 40 keV of 62.5 nm. somewhat larger than the TPP-2M value. The only other experimental measurement of the IMFP of Si_3N_4 at lower energies seem to indicate that the actual IMFP is smaller than the TPP-2M value [12].

These samples (35 nm Si_3N_4 on TiO_2) were annealed at 800 °C and etched in HF. After an etching of 270 s there was still some

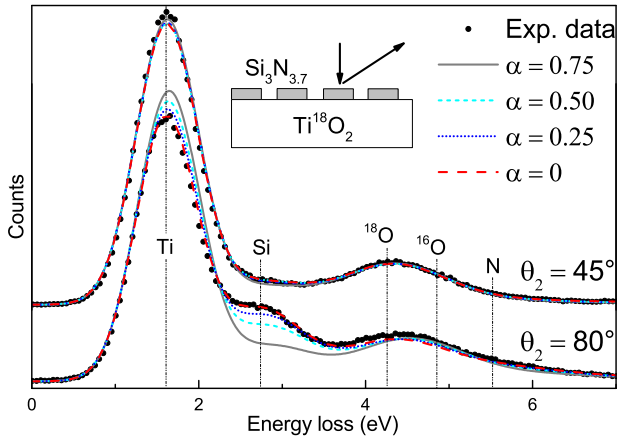

Fig. 6. The spectra of Si_3N_4 on TiO_2 after etching. The spectra are now dominated by TiO_2. For the calculations it was assumed that the sample was covered with patches of Si_3N_4, with all patches having the same thickness. A fraction α of the surface was assumed not covered by Si_3N_4. The distribution of the Si_3N_4 affects the measurements with $\theta_2 = 80^\circ$, but the best fit is obtained if one assumes a homogeneous distribution.

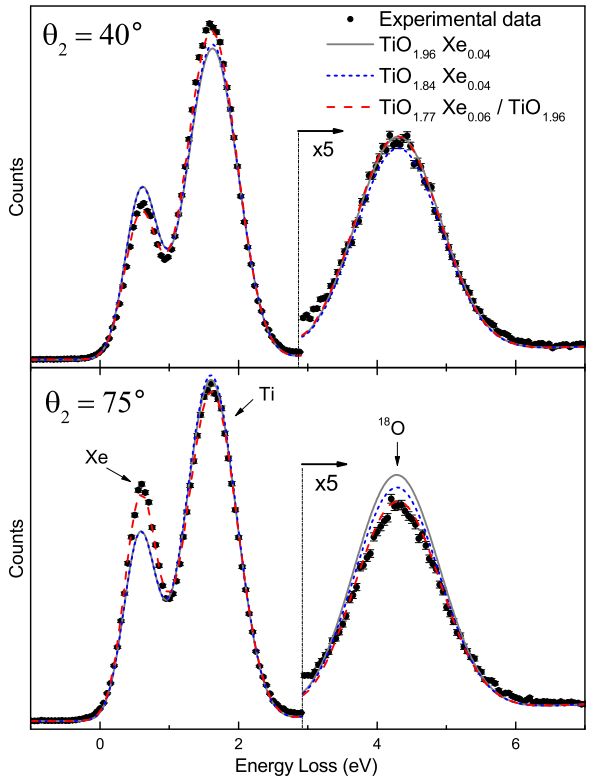

Fig. 7. Two ERBS spectra taken in different geometries of a TiO_2 sample sputtered with 3 keV Xe ions as well several fits based on simple assumptions of the Xe and O depth distributions as described in the main text. The energy E_0 was 40 keV.

Si_3N_4 visible in the ERBS spectra, an amount equivalent to what is expected for 3.6 nm (see Fig. 6). The question arises if the remaining Si_3N_4 forms a uniform layer or should be described by thicker patches surrounded by bare TiO_2. From a single ERBS spectrum one would never be able to tell this. By fitting two ERBS spectra simultaneously the situation could change due to the non-linear nature of Eqs. (1) and (2).

It was assumed that the sample was covered with patches of Si_3N_4, with all patches having the same thickness. A fraction α of the surface was assumed not covered by Si_3N_4. The spectrum taken with $\theta_2 = 45^\circ$ is determined by the total amount of Si_3N_4 present and is not very sensitive to the actual distribution of Si_3N_4. The spectrum taken in the surface sensitive geometry ($\theta_2 = 80^\circ$) is affected, as in this geometry the path length in the Si_3N_4 patches becomes comparable to the IMFP, especially for larger α values and hence thicker patches for a given amount of Si_3N_4. The best fit was obtained for $\alpha = 0$, i.e. there is no indication in our measurement of a non-uniform overlayer.

Our model covers of course not all possible surface structures, but it is clear that the Si_3N_4 should be fairly homogeneous distributed in order to be consistent with the measurement. This conclusion can only be drawn if one analyses two spectra with different degrees of surface sensitivity simultaneously. For $\alpha = 0$ the calculated line shape is slightly lower than the experiment in the glancing geometry for energy losses near 4.8 eV, the recoil energy of electrons scattering from ^{16}O. This could be a sign of some water absorbed on the surface, as the sample was not cleaned after insertion into the vacuum.

4.3. Xe sputtered TiO_2

Finally we want to describe an attempt of analysing an even more complicated case, a Xe sputtered TiO_2 film. The Xe sputtering was done with 3 keV Xe^+ ions directed along the surface normal. The projected range, as calculated by TRIM [13] under these conditions, is 3.8 nm with a noticeable Xe concentration extending up to 6 nm. Here the implanted Xe atoms will have a concentration that varies with depth. Also the stoichiometry of the outermost layer may have changed, due to preferential sputtering. Two spectra were obtained, one with $\theta_2 = 40^\circ$ (and hence the incoming beam close to the surface normal), and one with $\theta_2 = 75$ (incoming beam 30° away from the surface normal) (see Fig. 7). The peak due to the implanted Xe ions is clearly visible besides the peaks due to Ti and O. The TiO_2 film before implantation was analysed as well and we obtained from ERBS a stoichiometry of $TiO_{1.96}$. The variation in the relative Xe intensity indicates a non-uniform concentration of the sample with the more surface sensitive geometry detecting more Xe. Fitting the spectrum as a homogeneous sample consisting of $TiO_{1.96}$ and Xe one obtains 0.04 Xe atom per Ti atom but the fit does not describe both measurements well. For the surface sensitive geometry ($\theta_2 = 75^\circ$) the calculated O intensity is too high and the calculated Xe intensity is too low. For the bulk sensitive geometry ($\theta_2 = 40^\circ$) the calculated Xe intensity is too high, and the calculate Ti intensity too low.

Subsequently it was assumed that the O concentration was different after sputtering but the sample was still homogeneous. Now only a slightly better fit was obtained for a composition $TiO_{1.84}Xe_{0.04}$.

A good fit can only be obtained if one assumes that the sample consist of two (or more) layers. In the simplest two-layer model the sample consists of one layer (thickness t) of TiO_xXe_y and a substrate not affected by the sputtering of $TiO_{1.96}$. There are now three variables to fit: x, y and t. Using only one spectrum it is not possible to get unique values for x, y and t, but using both spectra and treating x, y and t as shared parameters we obtain a good fit with a thickness of 14 nm and a composition $TiO_{1.77}Xe_{0.06}$. Surprisingly this depth exceeds the Xe implantation range by more than a factor of 2. Of course the actual structure will have more gradual concentration changes as our model and with the depletion in oxygen not so simply related to the Xe concentration, but as the simple model describes our data well, we can not expect to resolve the depth distributions in more detail.

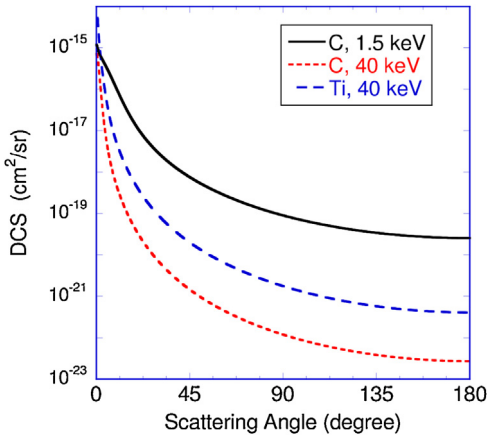

Fig. 8. The DCS of C at 1.5 keV and 40 keV, as well as the DCS of Ti at 40 keV.

5. Discussion and conclusion

In the previous sections we have shown that multi-layer ERBS spectra can be fitted successfully in a very simple way. The main question arises then if the extracted information is affected by any of the assumptions made, in particular the assumption of v-shaped trajectories, i.e. only a single large-angle scattering event. Multiple deflections will affect the measurement in two ways

- The recoil energy can differ, as now there is not a single collision with a well-defined scattering angle.
- The path lengths in the overlayer will be different and hence the attenuation by inelastic events will not follow the simple exponential decay described by the IMFP.

The first point was investigated previously by Monte Carlo simulation for the case of thick graphite films [8]. These simulations showed that trajectories with multiple deflections are much more common than trajectories with only a single deflection, but that almost always only one large-angle deflection dominates and multiple scattering causes only a slight increase in width of the peak. Those rare trajectories with multiple large-angle deflections will have different recoil losses and contribute to the background, rather than the peaks.

For E_0 = 1.5 keV Alvarez et al found, using Monte Carlo simulations, a 10% overestimation of the H content in polyethylene by ERBS [14]. We expect this effect to be even smaller for higher E_0 values. This is due to the shape of the DCS, as is shown in Fig. 8. The small effect Alvarez et al found on the shape of the spectrum, in spite of frequent occurrence of multiple scattering of mixed scattering from C and H (much more frequent than single scattering from H) is due to the shape of the cross section. The forward peaked nature of the DCS ensures that most of the mixed scattering events combine a small angle deflection from C (H) with a large angle deflection from H(C). The recoil loss is determined almost exclusively by the large angle deflection. Increasing E_0 to 40 keV makes the DCS even more strongly peaked at 0° and the tendency of one large-angle deflection to dominate after multiple scattering should be even stronger.

The second point has been well-studied in the context of XPS, where it is described as the difference between the effective attenuation length (EAL) and the inelastic mean free path. For a recent discussion see a recent paper by Jablonski and Penn [15]. It is generally accepted that the difference between effective attenuation length and the IMFP is related to the transport mean free path. The transport mean free path is given by

$$\lambda_{tr}^{-1} = N_a \int_{4\pi} (1 - \cos\theta_{scat}) \frac{d\sigma_e}{d\Omega} d\Omega \quad (4)$$

with N_a the density of atoms and σ_e the elastic scattering cross section λ_{tr} is associated with the distance in a material over which the direction of propagation of a particle is randomized. Especially for light elements and at multiple keV energies the elastic cross section is strongly peaked in the forward direction (where $(1 - \cos\theta_{scat}) \approx 0$) and the transport mean free path is much longer than either the elastic or inelastic mean free path. Under these conditions the difference between the IMFP and the EAL becomes small. For graphite at 40 keV the value calculated using ELSEPA of λ_{tr} is 16,700 nm, about 500 times larger than the IMFP. At 20 keV λ_{tr} is 4780 nm. For Si_3N4 λ_{tr} is 6590 nm at 40 keV. The transport mean free path are two orders of magnitude larger here than the IMFP, and hence the error introduced by assuming v-shaped trajectories should be very small indeed. On close inspection the argument in this paragraph is very similar to the argument in the preceding paragraph.

In summary we have shown that for multi-layered samples we can calculate the ERBS spectra well, and describe spectra obtained under different experimental conditions quantitatively with a single set of input parameters. The only adjustments made in obtaining the quantitative comparison have to do with the shape of the (low-intensity) background, and some experimental parameters, such as energy resolution and exact zero position of the energy scale. This further establishes the capabilities of ERBS as a technique to analyse samples at depths an order of magnitude larger than can be done by laboratory-based XPS.

Acknowledgements

This work was realized with support from CNPq, Conselho Nacional de Desenvolvimento Científico e Tecnológico – Brazil and the Australian Research Council.

Appendix A. Supplementary Data

Supplementary data associated with this article can be found, in the online version, at http://dx.doi.org/10.1016/j.elspec.2015.02.009.

References

[1] M. Went, M. Vos, Appl. Phys. Lett. 90 (2007) 072104.
[2] M. Went, M. Vos, Nucl. Instr. Methods Phys. Res. Sect. B 266 (2008) 998.
[3] M. Vos, K. Tokesi, I. Benko, Microsc. Microanal. 19 (2013) 576.
[4] F. Salvat, Phys. Rev. A 68 (2003) 012708.
[5] F. Salvat, A. Jablonski, C.J. Powell, Comput. Phys. Commun. 165 (2005) 157.
[6] S. Tanuma, C.J. Powel, D.R. Penn, Surf. Interface Anal. 20 (1993) 77.
[7] S. Tanuma, C.J. Powell, D.R. Penn, Surf. Interface Anal. 43 (2011) 689.
[8] M. Vos, R. Moreh, K. Tőkési, J. Chem. Phys. 135 (2011) 024504.
[9] M. Vos, M.R. Went, Surf. Sci. 601 (2007) 1536.
[10] M. Vos, P. Storer, Y.Q. Cai, I.E. McCarthy, E. Weigold, Phys. Rev. B 51 (1995) 1866.
[11] S. Tanuma, C. Powell, D. Penn, Surf. Interface Anal. 17 (1991) 911.
[12] R. Jung, J. Lee, G. Orosz, A. Sulyok, G. Zsolt, M. Menyhard, Surf. Sci. 543 (2003) 153.
[13] J.F. Ziegler, Nucl. Instr. Methods Phys. Res. Sect. B: Beam Interact. Mater. Atoms 219–220 (2004) 1027.
[14] R. Alvarez, F. Yubero, Surf. Interface Anal. 46 (2014) 812.
[15] A. Jablonski, C. Powell, J. Electron Spectrosc. Relat. Phenom. 199 (2015) 27.